Journal of Medicinal Chemistry

Article

pubs.acs.org/jmc

Highly Potent and Selective Fluorescent Antagonists of the Human Adenosine A_3 Receptor Based on the 1,2,4-Triazolo[4,3-*a*]quinoxalin-1-one Scaffold

Andrea J. Vernall,[†] Leigh A. Stoddart,[‡] Stephen J. Briddon,[‡] Stephen J. Hill,*[,‡] and Barrie Kellam*[,†]

[†]School of Pharmacy, Centre for Biomolecular Sciences, University of Nottingham, United Kingdom

[‡]Institute of Cell Signalling, School of Biomedical Science, Queen's Medical Centre, University of Nottingham, United Kingdom

ABSTRACT: The adenosine-A_3 receptor (A_3AR) is a G protein-coupled receptor that shows promise as a therapeutic target for cancer, glaucoma, and various autoimmune inflammatory disorders, and as such, there is a need for molecular probes to study this receptor. Here, we report a series of fluorescent ligands containing different linkers and fluorophores based around a 1,2,4-triazolo[4,3-*a*]quinoxalin-1-one antagonist. One of these conjugates (**19**) displayed high affinity for the A_3AR (pK_D = 9.36 ± 0.12) and is >650-fold selective over other adenosine receptor subtypes. Confocal microscopy revealed clear, displaceable membrane labeling of CHO-A_3 cells with **19**, with no detectable labeling of CHO-A_1 cells under identical conditions. This fluorescent ligand was also able to specifically label the A_3AR in HEK293T cells containing a mixed adenosine receptor population. The subtype specificity, along with its excellent imaging properties, make **19** an ideal tool for studying A_3AR distribution and organization, particularly in the presence of other adenosine receptor subtypes.

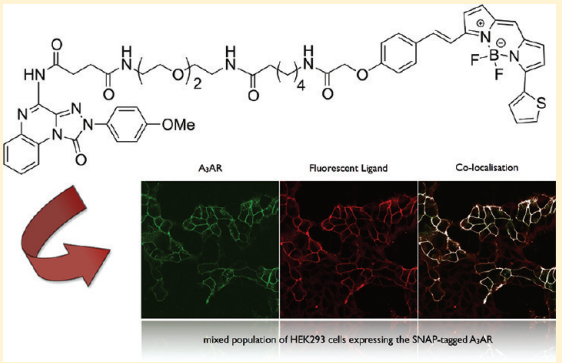

INTRODUCTION

G protein-coupled receptors (GPCRs) are the largest family of transmembrane signaling proteins in the human genome and are estimated to be the target of around 40% of all currently marketed drugs. Structurally, GPCRs consist of seven transmembrane spanning helices linked via intra- and extracellular loop regions, and their cell signaling is critical to a vast array of physiological processes.[1] Within the GPCR superfamily, there are four adenosine receptors (AR) that bind and are activated by the purine nucleotide. There are four characterized AR subtypes, the A_1AR, A_{2A}AR, A_{2B}AR, and the larger A_3AR. The A_3AR is the least characterized of the receptor subtypes and is more commonly found in peripheral tissues such as lung and liver, yet also in immune cells such as mast cells and neutrophils.[2]

The A_3AR is increasingly being implicated in many biological processes and diseases, registering this receptor as a therapeutic target worthy of further study,[3,4] with both agonist and antagonist A_3AR ligands showing potential as therapeutic agents and diagnostic tools.[5] For example, A_3AR agonists have been evaluated for the treatment of autoimmune inflammatory diseases such as rheumatoid arthritis, psoriasis, and dry-eye disease[6] and for liver cancer.[7] A_3AR activation by a subtype-selective agonist has also been shown to have a cardioprotective effect in ischemic myocardium.[8] Receptor inactivation by an A_3AR antagonist is being considered as a treatment for glaucoma.[9] Several tumor cell lines have been shown to contain elevated levels of A_3ARs, with the expression level thought to correlate to the tumor stage and severity.[10] In particular, for colon cancer, the A_3AR has been proposed as a diagnostic marker for tumorigenesis and disease progression.[11] With the increasing importance of the A_3AR as a therapeutic target comes a requirement for biological tools to study this receptor. To fill this need, herein, we report a highly potent and selective fluorescent antagonist (**19**) that can specifically bind to the A_3AR in a cell line that endogenously expresses multiple AR subtypes.

Using fluorescence as a means to study GPCRs allows access to a large range of pharmacological techniques that can capture dynamic processes involving unmodified receptors in live cells.[12] In particular, fluorescently labeled ligands that act as an agonist or antagonist have been developed to target many GPCRs.[12,13] Visualization of a GPCR using a fluorescent ligand is a very sensitive technique, and measurements can be made at the single cell level; therefore, large numbers of cells are not required. Through the use of confocal microscopy, a fluorescent ligand can give real-time spatial information about dynamic protein−protein interactions, trafficking, localized expression level, and the mobility of the receptor. This is important as GPCRs are not uniformly distributed on the cell membrane but are organized into microdomains such as membrane rafts and caveolae.[14] Information about receptor mobility and its conformation can also be studied, for example, by using fluorescent correlation spectroscopy.[15] Fluorescent ligands also offer advantages over radioligands in competitive binding

Received: December 21, 2011
Published: January 25, 2012

assays,[16] as there are health risks and legal and disposal costs associated with radioactivity. In addition, there is currently no commercially available radiolabeled antagonist for the A_3AR.

There are examples of fluorescently labeled ligands that have been developed as biological probes for the ARs.[17,18] Xanthine-based antagonists have been functionalized as fluorescent ligands[19,20] but were poorly selective between the AR subtypes. There are several examples of fluorescent antagonists that are selective for the A_{2A}AR,[21,22] but here, we report the first example of a fluorescent antagonist that is selective for the human A_3AR. To study the A_3AR in primary human cell lines, it is essential that a molecular probe is exquisitely subtype selective, as nearly every mammalian cell expresses one or more of the AR subtypes.

There are several factors that must be considered when appending a fluorophore to a relatively small pharmacophore, as opposed to a peptide or protein. Both the linker type and length that separates the pharmacophore from the fluorophore and the fluorophore itself can affect the pharmacology of the final conjugate.[20] The linker must be attached to the pharmacophore in a position that is relatively insensitive to structural modification and that can tolerate bulky substituents. For a GPCR probe, the physiochemical properties of the final conjugate must be considered to minimize nonspecific membrane binding and/or prevent high intracellular ligand accumulation. Additionally, from an imaging perspective, the choice of fluorophore based on the adsorption/emission profile should be matched to the end biological application of the fluorescent ligand. In this study, we selected fluorophores that emit at a wavelength of 550−650 nm, as this does not overlap with cellular autofluorescence and allows colocalization studies with receptors tagged with fluorescent proteins (for example, YFP and GFP) to be carried out. The boron dipyrromethene scaffold has proven particularly useful in many biological imaging studies due to the excellent stability and photophysical properties of this fluorophore.[23]

A variety of chemical structures have been discovered that show selective A_3AR antagonism.[24] We chose trizoloquinoxalin-1-one **1**,[25] a selective A_3AR antagonist, as the pharmacophore starting point for congener assembly (Figure 1). Lenzi and co-workers have shown that a 4-methoxy group on the 2-phenyl ring and acylation of the 4-amino group instill a degree of A_3AR subtype selectivity to this compound family, for example, the 4-benzamido (**2**) (K_i = 2.9 ± 0.13 nM) and 4-acetamido (**3**) (K_i = 35.7 ± 2.40 nM) derivatives (Figure 1).[26] In addition, further structure−activity relationships have demonstrated that receptor affinity can be maintained when bulky functional groups are added to the 4-amino group of **1**.[27] Consequently, acylation of this 4-amino group was chosen as the method for linker attachment, meaning **1** could be readily synthesized as a common intermediate. Our goal therefore was not to further optimize the quinoxalin-1-one scaffold as an antagonist but rather to produce a fluorescent ligand that displayed a maintained potency and selectivity profile to the parent drug molecule.

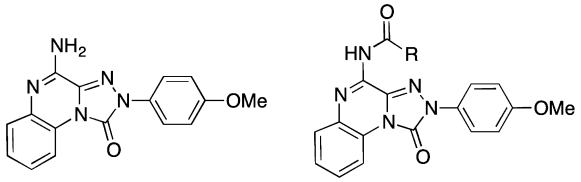

Figure 1. Previously reported 1,2,4-triazolo[4,3-*a*]quinoxalin-1-one derivatives.[25,26]

RESULTS AND DISCUSSION

Synthesis. Drawing upon previous successes, we sought to develop congeners equipped with both short and long linker variants of differing physiochemical properties. For the linear hydrocarbon and polyether variants, monoprotected diamines **4** and **5** were acylated with succinic anhydride to afford amides **6** and **7** in excellent yields (Scheme 1). Quinoxalin-1-one **1**[25] was then coupled to either **6** or **7** in the presence of 2-(1*H*-7-azabenzotriazol-1-yl)-1,1,3,3-tetramethyluronoium hexafluorophosphate (HATU)/1-hydroxy-7-azabenzotriazole (HOAt) in DMF to afford the protected congeners **10** and **11**, respectively. *tert*-Butyl carbamate (Boc)-Gly-OH (**8**) was coupled to **1** to afford **12**, while coupling the quinoxalin-1-one with benzyl carbamate (CBZ)-protected 4-amino benzoic acid (**9**) generated **13**. The Boc protecting groups of **10**, **11**, and **12** were subsequently removed using trifluoroacetic acid to give **14**, **15**, and **16**, respectively. The Cbz protecting group of **13** was removed by hydrogenolysis using 10% palladium-on-carbon and hydrogen to afford the 4-amino benzoyl derivative **17**.

The quinoxalin-1-one congeners (**14**−**17**) were then coupled to a range of commercially available fluorescent probes (Scheme 2). 6-(((4,4-Difluoro-5-(2-thienyl)-4-bora-3*a*,4*a*-diaza-*s*-indacene-3-yl)styryloxy)acetyl)amino hexanoic acid (BODIPY-X-630/650)-succinimidyl ester (SE) was reacted with amines **14** and **15** to give conjugates **19** and **18**, respectively. The polyether congener (**14**) was additionally coupled to 6-(((4-(4,4-difluoro-5-(2-thienyl)-4-bora-3*a*,4*a*-diaza-*s*-indacene-3-yl)phenoxy)acetyl)amino)hexanoic acid (BODIPY-X-TR)-SE, 3*H*-indolium,2-[5-[1-[6-[(2,5-dioxo-1-pyrrolidinyl)oxy]-6-oxohexyl]-1,3-dihydro-3,3-dimethyl-5-sulfo-2*H*-indol-2 ylidene]-1,3-pentadien-1-yl]-1-ethyl-3,3-dimethyl-5-sulfopotassium salt (Cy5-X)-SE, 6-(tetramethylrhodamine-5-(and-6)-carboxamido)hexanoic acid (TAMRA-5/6-X)-SE, and 5-TAMRA-polyethylene glycol (PEG)-SE to afford the fluorescent derivatives **20**−**23**. Attempts to couple the succinimidyl activated fluorophores to either **16** or **17** were regrettably unsuccessful, with both of these two congeners suffering from very poor organic solvent solubility; however, the extended linkers housed on congeners **14** and **15** helped obviate this solubility issue. All fluorescent ligands were initially isolated and purified using preparative reversed-phase high-pressure liquid chromatography (RP-HPLC); their final purity was confirmed using RP-HPLC with dual wavelength detection with the compound identity subsequently confirmed by HRMS (TOF ES+). The purities of all compounds subsequently tested in biological systems were determined as being ≥95%.

Pharmacology: Functional Studies. To initially address whether this novel series of fluorescent ligands were able to antagonize agonist-stimulated responses at the A_3AR, we evaluated their capacity to attenuate functional activity in Chinese hamster ovary (CHO) cells, which expressed both the target receptor alongside a six cyclic adenosine monophosphate (cAMP) response element (6 CRE) promoter driving the expression of a human-secreted placental alkaline phosphatase reporter gene.[28] All of the quinoxalin-1-one congeners, alongside their respective fluorescent conjugates, were able to

Scheme 1. Synthesis of Quinoxalin-1-one Congeners[a]

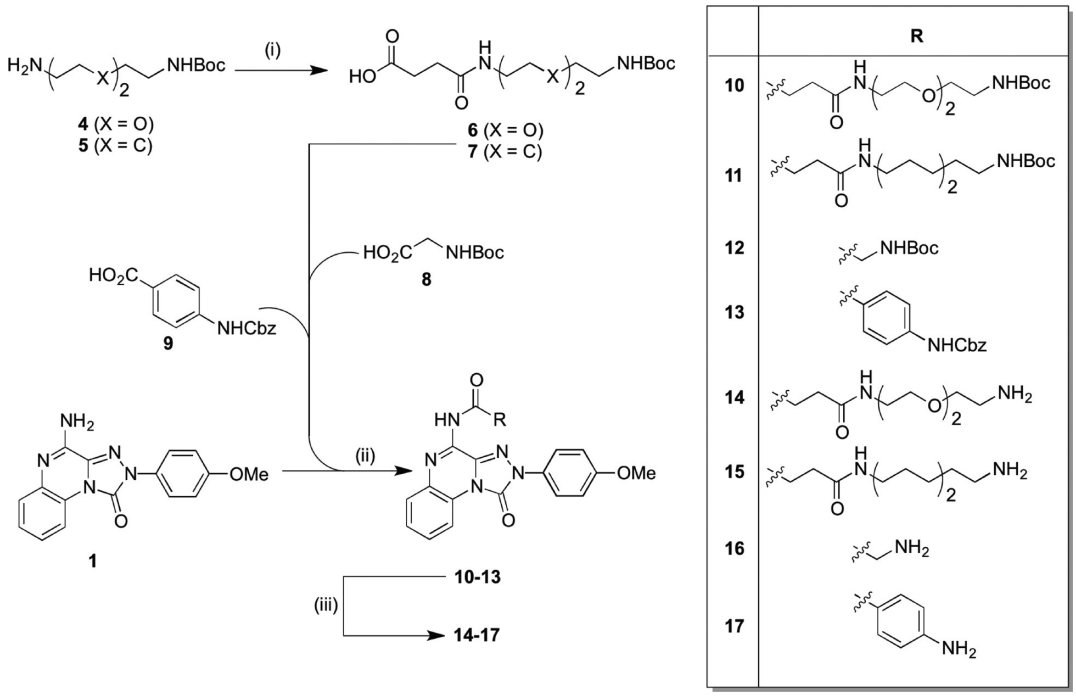

[a]Reagents and conditions: (i) Succinic anhydride, $CHCl_3$, 0 °C and then 12 h room temperature, 82−95%. (ii) HATU, HOAt, *N*,*N*-diisopropylethylamine, DMF, carboxylic acid (**6**, **7**, **8**, or **9**), 18 h, 10−67%. (iii) For **10**−**12**, trifluoroacetic acid, CH_2Cl_2, 1 h, quantitative; for **13**, 10% Pd/C, H_2, MeOH/H_2O/acetic acid, 3 h, quantitative.

antagonize the adenosine-5-*N*-ethylcarboxamide (NECA)-mediated agonist response at the human A_3AR (Table 1), and of the fluorescent ligands tested, **19** and **20** displayed the highest affinity. Comparison of the literature binding affinities of the known antagonists **1**−**3** to our novel linker-modified ligands revealed that acyl extension from the 4-amino position of **1** was an amenable strategy for congener assembly (Table 1). The polyether variant **14** (pK_D = 7.68 ± 0.25; Table 1) proved to be the worst of the linker-modified compounds, yet still maintained a binding affinity similar to the native drug (**1**) (pK_D = 7.43 ± 0.13).[25] The binding affinity of aniline **17** was reduced 40-fold as compared to the benzoyl equivalent (**2**), demonstrating that introduction of a *p*-amino group is not advantageous as a solitary chemical maneuver. The two most potent congeners were glycyl derivative **16** (pK_D = 8.84 ± 0.16; Table 1) and aminooctanoyl derivative **15** (pK_D = 9.48 ± 0.16; Table 1). The former displayed a small affinity enhancement over the simple acetamido analogue **3** and a similar affinity to **2**, whereas the latter displayed a greater affinity than both **3** and **2**.

The binding affinities of **18**−**23** varied about 300-fold, demonstrating that the fluorophore exerts a major influence on the final pharmacology of the conjugate. We have previously established how the fluorophore component of both xanthine amine congener (XAC)- and NECA-based conjugates greatly influences the ultimate binding affinities at the A_1AR.[20] The C8-linked conjugate **18**, which contained the BODIPY 630/650-X moiety, displayed a moderate affinity at the A_3AR (pK_D = 7.78 ± 0.16); however, this represented a 40-fold reduction in affinity when compared to the precursor congener **15**. Five fluorescent ligands (**19**−**23**) were synthesized from PEG-linked **14**, of which the BODIPY 630/650-X variant (**19**) showed excellent affinity (pK_D = 9.36 ± 0.12) at the A_3AR, acting as a competitive antagonist (Figure 2a). This was extremely rewarding, since this was an increase on the already high affinity of the benchmark quinoxalin-1-one **2** and suggested that the BODIPY 630/650 scaffold must be contributing in a favorable way to the binding affinity of **19**, as it was significantly better than the PEG-linked congener **14**. However, the interplay of contributing factors is complicated; if it were simply the BODIPY 630/650 that was responsible for the increase in affinity, then one would not unreasonably expect the binding affinity of C8-linked **18** to also be better than the corresponding congener **15**. There is a 40-fold difference in binding affinity between conjugates **18** and **19** that differ only by the replacement of two methylenes with an ether oxygen, indicating that the linker is also contributing to the overall conjugates pharmacology. Comparing the congener−conjugate pairs, there is an 80-fold increase in affinity going from the PEG-linker compound **14** to the corresponding fluorescent conjugate **19**, while from the analogous C8-linker **15** to C8 fluorescent conjugate **18**, there is a overall 40-fold decrease in binding affinity.

PEG-linked conjugate **20**, which contained the BODIPY-TR fluorophore, also acted competitively as a high-affinity antagonist at the A_3AR (pK_D = 8.47 ± 0.16, Figure 2b). The only structural difference between **19** and **20** is that the former contains an ethenyl spacer between the borondipyrromethane scaffold and the connecting phenyl group; yet, this imparts an 8-fold difference in activity. This would suggest that the BODIPY component of **18**, **19**, and **20** is likely engaging in specific interactions with the A_3AR and is not simply acting as a membrane anchor or protruding unbound into the extracellular environment. Replacing the BODIPY 630/650 of **19** with a Cy5 fluorophore to give **21** resulted in a 300-fold reduction in A_3AR affinity. This reiterates the large contribution that the fluorophore has to conjugate binding, as **19** and **21** contain the

dx.doi.org/10.1021/jm201722y | *J. Med. Chem.* 2012, 55, 1771−1782

Scheme 2. Synthesis of Fluorescent A_3AR Antagonists[a]

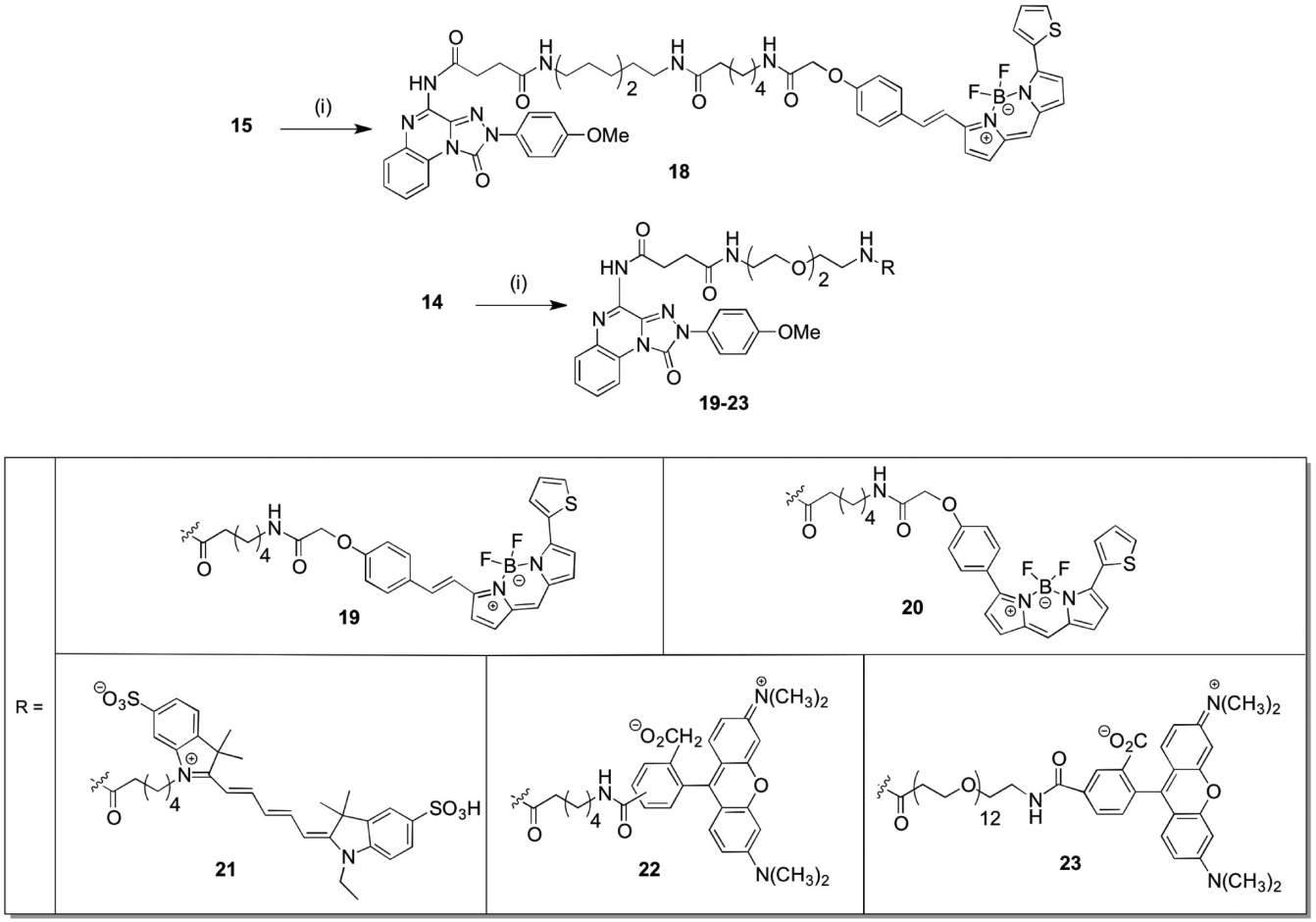

[a]Reagents and conditions: (i) Fluorophore-SE, *N*,*N*-diisopropylethylamine, DMF, 22−60% yield after RP-HPLC purification.

Table 1. Binding Affinities of 1,2,4-Triazolo[4,3-*a*]quinoxalin-1-one Derivatives at Human A_3AR

compd	hA$_3$AR pK_D[a]	*n*
14	7.68 ± 0.25	9
15	9.48 ± 0.16	3
16	8.84 ± 0.16	6
17	7.42 ± 0.23	8
18	7.78 ± 0.16	4
19	9.36 ± 0.12	6
20	8.47 ± 0.16	4
21	6.83 ± 0.05	3
22	7.53 ± 0.11	3
23	8.25 ± 0.16	3

[a]pK_D values were obtained from Gaddum shifts of FSK-stimulated CRE-SPAP responses to NECA in CHO cells expressing the human A_3AR. Values are means ± SEMs for *n* separate experiments.

same pharmacophore and linker. Conjugate **22**, which contained the charged TAMRA moiety, showed similar activity to precursor **14** and displayed significantly higher affinity than the charged Cy5 conjugate **21**. To study the effect of moving the charged fluorophore component of the ligand further away from the quinoxalin-1-one core, the extended PEG-linked **23** was synthesized. Conjugate **23** was 5-fold more active than **22**, indicating that in this case an increased distance between the TAMRA and the quinoxalin-1-one core improved overall binding.

The two highest affinity fluorescent conjugates **19** and **20** were also assayed for their ability to antagonize the A_1 and A_{2B} ARs (Table 2 and Figure 2). Affinity values at the A_1AR were measured in CHO cells expressing the human form of the A_1AR receptor, where an agonist-stimulated increase in intracellular calcium was measured, and the ability of a single concentration of **19** or **20** to shift these NECA concentration response curves was analyzed. As with the A_3AR, both **19** and **20** acted as competitive A_1AR antagonists but with appreciably lower affinities (Figure 2c,d). This revealed that **19** has a 650-fold increase in affinity and **20** a 50-fold higher affinity at the A_3AR over the A_1AR. Affinity values at the A_{2B}AR were measured in human embryonic kidney 293 (HEK293) cells that endogenously express the human A_{2B}AR and coexpressed the Glosensor cAMP biosensor. HEK293 cells were again stimulated with the AR agonist NECA, and the resulting increase in cAMP was measured. The shifts in the agonist concentration−response curves in the presence of **19** or **20** were used to estimate the affinity at the A_{2B}AR. At relatively high concentrations (1 mM), both **19** and **20** were unable to cause a significant shift in the NECA concentration response curve, indicating very low affinity at the A_{2B} AR.

Confocal Microscopy. While an excellent binding affinity and A_3AR subtype selectivity is a key prerequisite for a high-quality fluorescent ligand, this does not necessarily translate

dx.doi.org/10.1021/jm201722y | *J. Med. Chem.* 2012, 55, 1771−1782

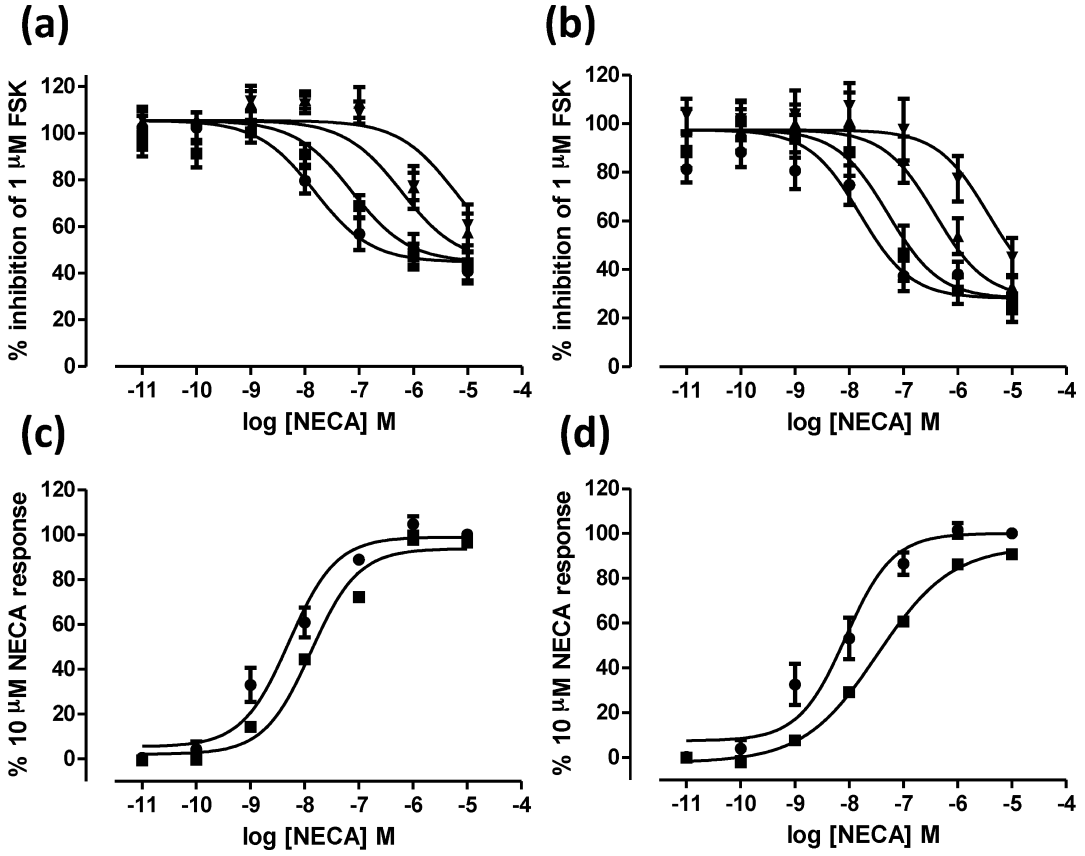

Figure 2. Functional analysis of fluorescent ligands **19** and **20** at A_3AR and A_1AR. (a and b) A_3AR-expressing CRE-SPAP cells were stimulated with 1 μM FSK and increasing concentrations of the agonist NECA (●). The ability of 10 nM (■), 100 nM (▲), and 1 μM (▼) **19** (a) or **20** (b) to inhibit the NECA response was analyzed. Data are normalized to basal (in the absence of FSK) and 1 μM FSK SPAP production. (c and d) A_1AR-expressing CHO cells were stimulated with increasing concentrations of NECA, and the resulting increase in calcium was measured (●). The ability of 1 μM (■) **19** (c) and **20** (d) to inhibit the NECA response was analyzed. The data shown represent the mean ± SEM of eight (a and c), four (b), and six (d) experiments performed in triplicate.

Table 2. Binding Affinities of Fluorescent 1,2,4-Triazolo[4,3-*a*]quinoxalin-1-one Conjugates 19 and 20 at Human A_3, A_1, and A_{2B} ARs

compd	hA$_3$AR pK_D[a]	hA$_1$AR pK_D[b]	hA$_{2B}$AR pK_D[c]	*n*
19	9.36 ± 0.12	6.56 ± 0.1	>6	6
20	8.47 ± 0.16	6.78 ± 0.13	>6	4

[a]Measured by the shift of NECA-mediated inhibition of FSK-stimulated CRE-SPAP response in CHO cells expressing the human A_3AR. [b]Measured by inhibition of increases in calcium induced by NECA in CHO cells expressing the human A_1AR. [c]Measured by the inhibition of increase in cAMP induced by NECA as determined by a cAMP biosensor in HEK293 cells that endogenously express the human A_{2B}AR.

into an effective biological probe for optical-based experiments. The physiochemical and photochemical properties of the ligand must also be suitable; the final conjugate must bind to the A_3AR with little or no nonspecific membrane binding and should not diffuse into the cell cytosol in large amounts. Fluorescent ligands **19** and **20** were examined using confocal microscopy for their ability to bind to CHO cells stably expressing either the human A_3AR or A_1AR (Figure 3).

The confocal microscope images of fluorescent ligands **19** and **20** with CHO-A_3 cells (Figure 3a,b) show localized membrane fluorescence and very little intracellular fluorescence. When cells were pretreated with *N*-[9-chloro-2-(2-furanyl)[1,2,4]-triazolo[1,5-*c*]quinazolin-5-yl]benzene acetamide (MRS1220), a nonfluorescent selective A_3AR antagonist, the specific-membrane fluorescence was substantially reduced in cells treated with **19**, although low levels of membrane-localized fluorescence was still present in cells treated with **20**, indicating that the majority of the membrane fluorescence observed is specific labeling of the A_3AR. The ability of **19** and **20** to bind to CHO-A_1 cells was also examined using confocal microscopy, to see if the difference in measured binding affinity at A_1AR is reflected in the degree of observed ligand−receptor binding. Low levels of fluorescence were observed when CHO-A_1 cells were treated with 25 nM (Figure 3a) and even up to 100 nM (data not shown) of **19**, and there was very little membrane localization of the fluorescence. Pretreatment of the CHO-A_1 cells with the nonfluorescent A_1AR selective antagonist 8-cyclopentyl-1,3-dipropylxanthine (DPCPX) before addition of **19** had little effect on the location and level of the observed fluorescence. This indicated that, at these concentrations, binding of **19** to the A_1AR was negligible. In line with the functional selectivity data, treatment of CHO-A_1 cells with 25 nM **20** (Figure 3b) resulted in a small amount of localized membrane fluorescence, which could only be partially displaced when the cells were pretreated with the A_1AR antagonist DPCPX. This suggests that **20** has some nonspecific binding to CHO cell membranes, but in cells expressing A_3AR, the levels of specific binding are high enough to allow it to be easily distinguished from nonspecific binding.

dx.doi.org/10.1021/jm201722y | *J. Med. Chem.* 2012, 55, 1771−1782

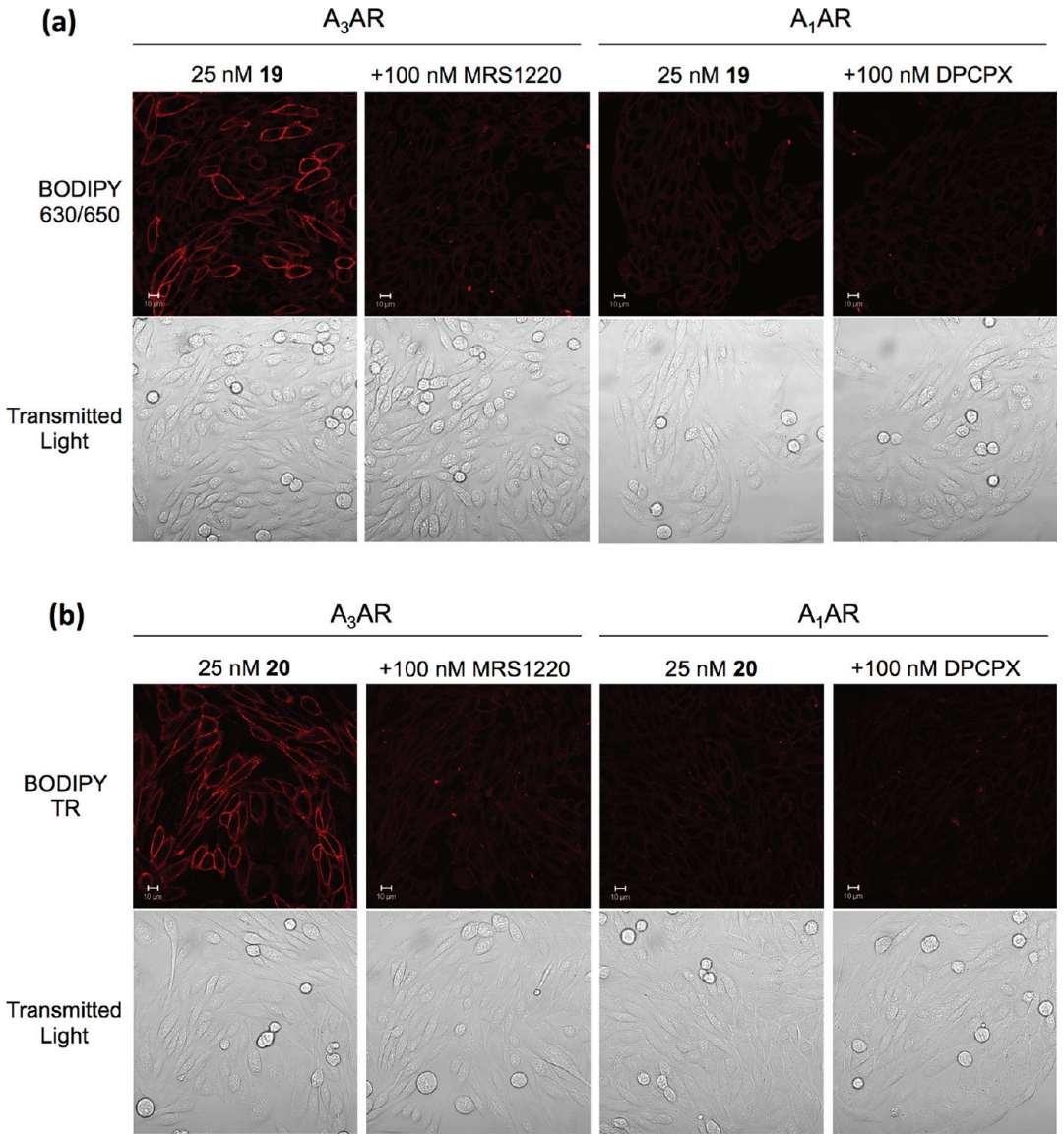

Figure 3. Visualization of the binding of (a) **19** and (b) **20** on CHO cells expressing A_3AR (left-hand panels) or A_1AR (right-hand panels). In each case, the upper row of images shows a confocal image, while the bottom row shows the transmitted light image of the same field of cells. In all conditions, cells were incubated for 30 min at 37 °C in the presence or absence of 100 nM of either MRS1220 or DPCPX followed by a 10 min incubation with a 25 nM concentration of the required fluorescent conjugate. Single equatorial confocal images were then obtained in the continued presence of the fluorescent ligand and/or unlabeled antagonist. For each fluorescent ligand, images were obtained using identical settings for laser power and detector offset and gain, as described in the Experimental Section. Images shown are from a single experiment representative of 3−5 performed.

Selectivity of fluorescent probes for the A_3AR is particularly important when attempting to observe and measure the receptor in native systems, where it is often expressed along with the A_{2A} or A_{2B}AR subtypes. We therefore investigated the ability of **19** to bind specifically to the A_3AR in the presence of A_{2B} receptors using HEK293 cells, which express the A_{2B}AR endogenously.[29] A mixed population of these cells transfected to express the human A_3AR, tagged on its N terminus with the sig-SNAP-tag,[30] were incubated with **19** (5 nM) in the presence and absence of the A_3AR antagonist MRS1220 (Figure 4).

As depicted in Figure 4, clear membrane binding of **19** was seen in HEK293 cells that expressed the sigSNAP-A_3AR. Cells in the same field of view that did not express the receptor (examples indicated in Figure 4 by the black arrow) showed no membrane labeling, indicating specific labeling of the A_3AR in these experiments. Such nonexpressing cells did, however, show some intracellular accumulation of ligand. Specificity of labeling was further confirmed in cells that had been pre-exposed to the nonfluorescent, high-affinity, A_3AR-selective antagonist, MRS1220 (100 nM), where membrane binding from A_3AR-expressing cells was clearly displaced. Similar experiments using the A_{2B}AR-selective antagonist 8-[4-[4-(4-chlorophenzyl)-piperazide-1-sulfonyl)phenyl]]-1-propylxanthine (PSB603) (100 nM) indicated no displacement of the binding of **19** from cells expressing the A_3AR or any changes in binding in cells not expressing the A_3AR (i.e., only the A_{2B}AR). Together, these results indicate that **19** will be of particular use in labeling the endogenous A_3AR in native tissues or cells, where coexpression of A_{2B}AR is a complicating factor.

dx.doi.org/10.1021/jm201722y | J. Med. Chem. 2012, 55, 1771−1782

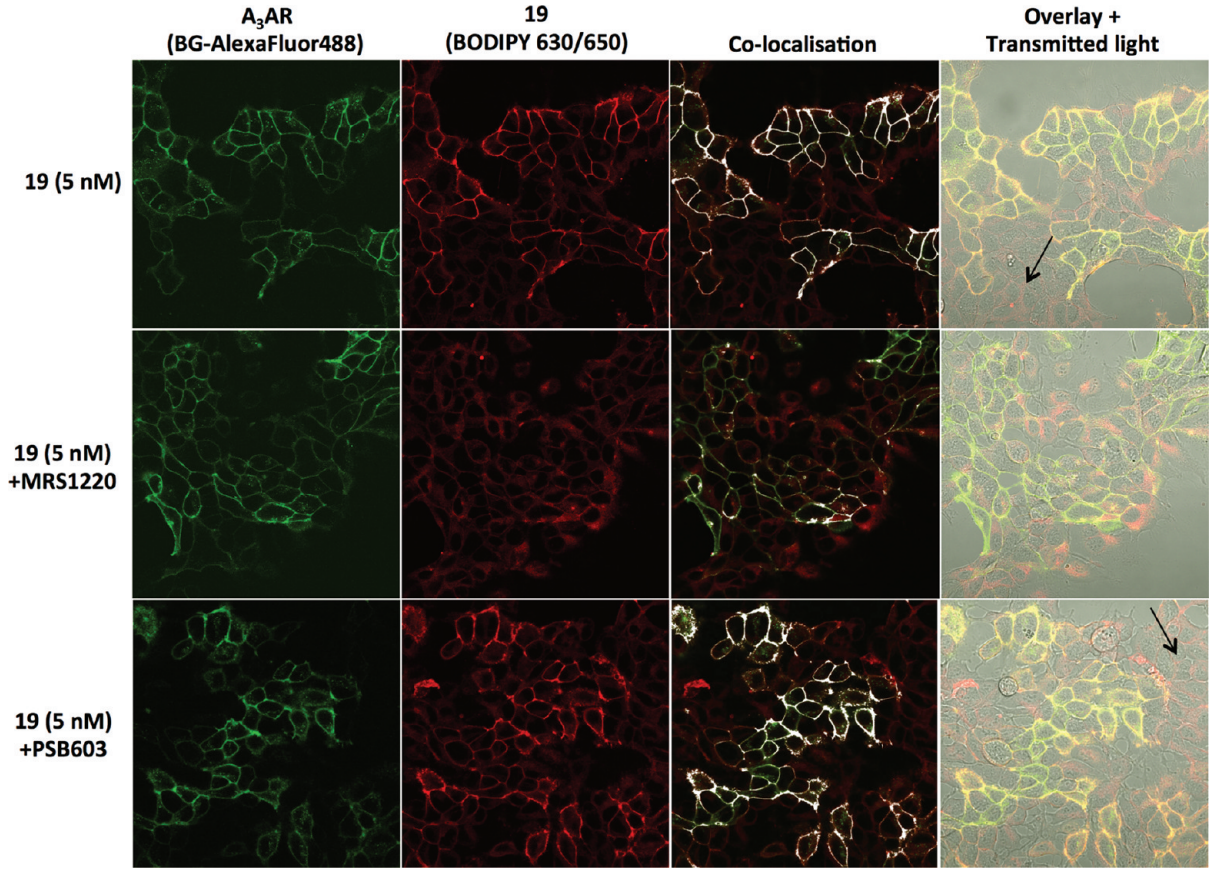

Figure 4. Binding of **19** to HEK293 cells expressing the sigSNAP-A_3AR. A mixed population of HEK293 cells expressing the SNAP-tagged A_3AR was incubated with **19** (5 nM, 10 min, room temperature) in the absence (top) or presence of MRS1220 (middle) or PSB603 (bottom; both 100 nM, 30 min, 37 °C). Single equatorial images were taken showing the BG-AlexaFluor488-labeled A_3AR (green) and **19** (red). Colocalized pixels of ligand and A_3AR (as determined by colocalizaiton analysis) are shown in white, as well as the fluorescent image overlaid onto a transmitted light image of the same cells. The black arrow indicates example cells in which there is little or no A_3AR expression. Data shown are representative of images taken in four independent experiments, with all images taken using identical settings for laser power, gain, and offset in both channels.

CONCLUSIONS

In this study, we have shown that the quinoxalin-1-one-based A_3AR antagonist **1** can be modified to include a linker and fluorophore, and for conjugate **19**, results in a fluorescent molecule displaying enhanced A_3AR binding affinity when compared to the native drug molecule, while maintaining excellent A_3AR subtype selectivity. As with our previously reported fluorescent ligands, the BODIPY moiety proved to be the superior fluorophore among our triazoloquinoxalin-1-one conjugates **18**–**23**. On the basis of selectivity and structure–activity relationships of the pharmacophore-linkers as compared to the final conjugates, the BODIPY moiety of **19** may be favorably interacting with different receptor residues as compared to the presumably orthosteric binding pocket occupied by the quinoxalin-1-one core. This could account for the very high A_3AR affinity of **19**. A similar hypothesis has previously been proposed by Tahtaoui et al., who identified Rhodamine and BODIPY-labeled pirenzepine antagonists of the human muscarinic M_1 receptor.[31] They suggested that there are different binding sites within the muscarinic M_1 receptor that accommodate the fluorophore and pirenzepine, with kinetic analysis revealing that fluorescent ligand dissociation is sensitive to treatment with a known allosteric modulator.[31] The possibility that **19** is interacting via a binding site extended from the classic orthosteric pocket is intriguing and certainly warrants further investigation. This study further demonstrates that designing a fluorescent conjugate with greater potency than the parent pharmacophore is an achievable outcome. At this juncture, molecular modeling studies have not yet been undertaken, as we believe binding interactions between the large and highly flexible **19** and an A_3AR homology model itself based on either rhodopsin[32] or the recently published A_{2A}AR[33−35] crystal structures may not be very informative, especially beyond the proposed quinoxalin-1-one binding pocket.[27]

Fluorescent conjugate **19** could, however, be used in the wider scientific community to identify and study the A_3AR in live cells that are involved in biological processes of interest. For example, **19** could be used to study the change in expression levels of A_3AR in disease states such as certain cancers, colocalization with other fluorescently tagged receptor types, and enable visualization of cell–cell interfaces where the A_3AR may be involved in cell signaling. In addition to an A_3AR identification tool, **19** could also be used in fluorescent correlation spectroscopy experiments or as a fluorescence ligand in a competitive binding assay to replace the more traditional radioligand-based approach.

EXPERIMENTAL SECTION

Chemistry: Materials and Methods. Chemicals and solvents of an analytical grade were purchased from commercial suppliers and used without further purification. BODIPY-630/650-X-SE, BODIPY-

dx.doi.org/10.1021/jm201722y | J. Med. Chem. 2012, 55, 1771–1782

TR-X-SE, and TAMRA5/6-X-SE were purchased from Molecular Probes (Invitrogen, United Kingdom). Cy5-X-SE was purchased from GE Healthcare UK Ltd. 5-TAMRA-PEG-SE was purchased from Cambridge Bioscience. Unless otherwise stated, reactions were carried out at ambient temperature. Reactions were monitored by thin-layer chromatography on commercially available precoated aluminum-backed plates (Merck Kieselgel 60 F254). Visualization was by examination under UV light (254 and 366 nm) or staining with $KMnO_4$ dip. Flash chromatography was performed using Merck Kieselgel 60, 230−400 mesh (Merck KgaA, Darmstadt, Germany) on a Biotage Flashmaster II system. NMR spectra were recorded on a Bruker-AV 400, ^1H spectra were recorded at 400.13 MHz, and ^{13}C NMR spectra were recorded at 101.62 MHz. Solvents used for NMR analysis (reference peaks listed) were DMSO-d_6 [$(C\underline{H}D_2)_2SO$ at δ_H 2.50 ppm, $(\underline{C}D_3)_2SO$ at 39.52 ppm] and $CDCl_3$ ($C\underline{H}Cl_3$ at δ_H 7.26 ppm, $\underline{C}DCl_3$ at 77.16). Chemical shifts (δ) are recorded in parts per million (ppm). Coupling constants (J) are recorded in Hz, and the significant multiplicities are described by singlet (s), doublet (d), triplet (t), quadruplet (q), broad (br), and multiplet (m). Spectra were assigned using appropriate COSY, DEPT, HSQC, and HMBC sequences. High-resolution mass spectra (HRMS)−time-of-flight, electrospray (TOF ES±) were recorded on a Waters 2795 separation module/micromass LCT platform. RP-HPLC was performed using a Waters 2767 sample manager and Waters 2525 binary gradient module and visualized at 254 and 366 nm with a Waters 2487 dual wavelength absorbance detector. Spectra were analyzed using MassLynx. Preparative RP-HPLC was performed using a Phenomenex Luna C8(2) 11A Axia F column (150 mm × 30 mm × 10 μm) at a flow rate of 20 mL/min. Semipreparative RP-HPLC was performed using a YMC-Pack C8 column (150 mm × 10 mm × 5 μm) at a flow rate of 3 mL/min. Analytical RP-HPLC was performed using a YMC-Pack C8 column (150 mm × 4.6 mm × 5 μm) at a flow rate of 1.0 mL/min. Analytical RP-HPLC was used to confirm that all final products were >95% pure. The retention time (R_t) of the final pure product is reported using an analytical RP-HPLC method of 0−2 min 10% solvent B in solvent A followed by a 2−25 min gradient of 10−90% solvent B in solvent A (solvent A = 0.05% TFA in H_2O, solvent B = 0.05% TFA in 9:1 v:v CH_3CN:H_2O).

***tert*-Butyl 2-(2-(2-Aminoethoxy)ethoxy)ethylcarbamate (4).** Compound **4** was synthesized according to the literature.[36]

***tert*-Butyl 8-Aminooctylcarbamate (5).** Compound **5** was synthesized according to the literature.[37]

General Procedure A: Synthesis of 6 and 7 via Acylation with Succinic Anhydride. To the monoprotected amine **4** or **5** (4−7 mmol) in chloroform (20 mL) at 0 °C was added succinic anhydride (1 equiv, 4−7 mmol). The solution was warmed to ambient temperature and stirred for 12 h. The solvent was evaporated under reduced pressure to afford the desired product.

*5,14-Diaza-17,17-dimethyl-4,15-dioxo-8,11,16-trioxaoctadecanoic Acid (**6**).* *tert*-Butyl 2-(2-(2-aminoethoxy)ethoxy)ethylcarbamate (**4**) gave **6** (1.14 g, 3.3 mmol, 82% yield) as a colorless oil. ^1H NMR ($CDCl_3$): δ 1.43 (s, 9H, $C(CH_3)_3$), 2.50 (m, 2H, CH_2), 2.67 (m, 2H, CH_2), 3.32 (m, 2H, CH_2), 3.54 (m, 2H, CH_2), 3.51−3.56 (m, 4H, CH_2), 3.60−3.61 (m, 4H, CH_2), 6.92 (br s, 1H, NH), 7.44 (br s, 1H, NH). $C_{15}H_{27}N_2O_7$ $(M - H)^-$ calculated, 347.1818; found, 347.1887.

*5,14-Diaza-17,17-dimethyl-4,15-dioxo-16-oxaoctadecanoic Acid (**7**).* *tert*-Butyl 8-aminooctylcarbamate (**5**) (6.7 mmol) gave **7** (2.29 g, 6.7 mmol, quantitative) as a white solid. ^1H NMR (DMSO-d_6): δ 1.21−1.24 (m, 8H, CH_2), 1.35−1.37 (m, 13H, CH_2, $C(CH_3)_3$), 2.28 (m, 2H, CH_2), 2.40 (m, 2H, CH_2), 2.89 (m, 2H, CH_2), 3.00 (m, 2H, CH_2), 6.73 (m, 1H, NH), 7.77 (m, 1H, NH).

*4-(Benzyloxycarbonylamino)benzoic Acid (**9**).* To a solution of 4-aminobenzoic acid (1.5 mmol) and sodium bicarbonate (13 mmol) in water (5 mL) and dioxane (5 mL) was added benzyl chloroformate (1.5 mmol). The mixture was stirred for 4 h, water (2 mL) was added, and the mixture was stirred for 12 h. The solution was acidified to pH 3 with 1 M HCl, and the precipitate was filtered, washed, and dried to give **9** (375 mg, 1.4 mmol, 93% yield) as a white solid. ^1H NMR (DMSO-d_6): δ 5.18 (s, 2H, OCH_2), 7.35−7.45 (m, 5H, ArH), 7.58 (m, 2H, ArH), 7.87 (m, 2H, ArH), 10.15 (s, 1H, NH), 12.66 (br s, 1H, CO_2H).

General Procedure B: Synthesis of 4-Amido-2-(4-methoxyphenyl)-1,2,4-triazolo[4,3-*a*]quinoxalin-1-one Derivatives (10−13). The appropriate carboxylic acid (2 equiv), HATU (2 equiv), HOAt (2 equiv), and DIPEA (4 equiv) were dissolved in DMF (1 mL). This solution was added to a solution of 4-amino-2-(4-methoxyphenyl)-1,2,4-triazolo[4,3-*a*]quinoxalin-1-one (**1**)[25] (1 equiv) in DMF (2 mL). The mixture was stirred at 50 °C for 6 h and then treated with a solution of the carboxylic acid (2 equiv), HATU (2 equiv), HOAt (2 equiv), and DIPEA (4 equiv) in DMF (1 mL). The mixture was stirred at 50 °C for a further 12 h. Evaporation of the solvent under reduced pressure gave a residue that was purified using silica flash column chromatography, eluting with 1−8% MeOH/DCM.

*tert-Butyl N-2-{2-[2-(3-{[2-(4-Methoxyphenyl)-1-oxo-1H,2H-[1,2,4]triazolo[4,3-a]quinoxalin-4-yl]carbamoyl}propanamido)-ethoxy]ethoxy}ethylcarbamate (**10**).* 4-Amino-2-(4-methoxyphenyl)-1,2,4- triazolo[4,3-*a*]quinoxalin-1-one (**1**) (0.3 mmol) was treated twice with a solution of 14-diaza-17,17-dimethyl-4,15-dioxo-8,11,16-trioxaoctadecanoic acid (**6**) (0.6 mmol), HATU (0.6 mmol), HOAt (0.6 mmol), and DIPEA (1.2 mmol) to afford the title compound (16 mg, 0.03 mmol, 10% yield) as a pale green solid. ^1H NMR (DMSO-d_6): δ 1.36 (s, 9H, $C(CH_3)_3$), 2.45−2.50 (m, 4H, CH_2), 2.91 (t, 2H, J = 7.0 Hz, CH_2), 3.10 (m, 2H, $NHC\underline{H}_2$), 3.22 (m, 2H, $NHC\underline{H}_2$), 3.33−3.43 (m, 6H, CH_2), 3.82 (s, 3H, OCH_3), 6.76 (br m, 1H, $N\underline{H}CH_2$), 7.12 (m, 2H, ArH phenyl), 7.49 (m, 1H, ArH quinoxaline), 7.56 (m, 1H, ArH quinoxaline), 7.69 (d, 1H, J = 7.8 Hz, ArH quinoxaline), 7.95−7.99 (m, 3H, $N\underline{H}CH_2$, ArH phenyl), 8.70 (d, 1H, J = 8.1 Hz, ArH quinoxaline), 10.56 (s, 1H, N$\underline{H}$). ^{13}C NMR (DMSO-d_6): δ 28.22, 28.77, 29.71, 32.07, 38.63, 51.26, 55.43, 69.15, 69.46, 69.55, 77.58, 114.24, 114.31, 121.63, 125.52, 126.44, 127.60, 127.78, 130.19, 130.86, 133.85, 141.13, 148.08, 155.59, 157.78, 171.23, 171.50. HRMS calculated for $C_{31}H_{40}N_7O_8$ $(M + H)^+$, 638.2938; found, 638.2930. Analytical RP-HPLC R_t = 18.10 min.

*tert-Butyl N-8-(3-{[2-(4-Methoxyphenyl)-1-oxo-1H,2H-[1,2,4]-triazolo[4,3-a]quinoxalin-4-yl]carbamoyl}propanamido)-octylcarbamate (**11**).* 4-Amino-2-(4-methoxyphenyl)-1,2,4- triazolo-[4,3-*a*]quinoxalin-1-one (**1**) (0.35 mmol) was treated twice with a solution of 5,14-diaza-17,17-dimethyl-4,15-dioxo-16-oxaoctadecanoic acid (**7**) (0.8 mmol), HATU (0.8 mmol), HOAt (0.8 mmol), and DIPEA (1.2 mmol) to give **11** (45 mg, 0.07 mmol, 20% yield) as an off-white solid. ^1H NMR (DMSO-d_6): δ 1.21−1.24 (m, 8H, CH_2), 1.33−1.36 (m, 13H, CH_2, $C(CH_3)_3$), 2.44 (t, 2H, J = 7.9 Hz, CH_2), 2.85−2.92 (m, 4H, CH_2), 3.04 (m, 2H, CH_2), 3.82 (s, 3H, OCH_3), 6.74 (br m, 1H, $N\underline{H}CH_2$), 7.12 (m, 2H, ArH phenyl), 7.50 (m, 1H, ArH quinoxaline), 7.56 (m, 1H, ArH quinoxaline), 7.69 (d, 1H, J = 7.8 Hz, ArH quinoxaline), 7.86 (m, 1H, $N\underline{H}CH_2$), 7.96 (m, 2H, ArH phenyl), 8.71 (d, 1H, J = 8.1 Hz, ArH quinoxaline), 10.57 (s, 1H, N$\underline{H}$). ^{13}C NMR (DMSO-d_6): δ 28.25, 28.68, 28.74, 29.13, 29.44, 29.81, 32.16, 38.56, 39.73*, 55.41, 77.24, 114.26, 114.30, 121.69, 125.52, 126.43, 127.59, 127.76, 130.18, 130.85, 133.84, 141.13, 148.07, 155.54, 157.76, 170.84, 171.51. *Underneath the DMSO-d_6 solvent peak, the chemical shift derived from HSQC spectrum. HRMS calculated for $C_{33}H_{44}N_7O_6$ $(M + H)^+$, 634.3353; found, 634.3347.

*tert-Butyl N-([2-(4-Methoxyphenyl)-1-oxo-1H,2H-[1,2,4]triazolo-[4,3-a]quinoxalin-4-yl]carbamoylmethyl)carbamate (**12**).* 4-Amino-2-(4-methoxyphenyl)-1,2,4- triazolo[4,3-*a*]quinoxalin-1-one (**1**) (0.06 mmol) was treated twice with a solution of Boc-Gly-OH (**8**) (0.12 mmol), HATU (0.12 mmol), HOAt (0.12 mmol), and DIPEA (0.24 mmol) to give **12** (17 mg, 0.04 mmol, yield 67%) as a pale yellow solid. ^1H NMR (DMSO-d_6): δ 1.38 (s, 9H, $C(CH_3)_3$), 3.81 (s, 3H, OCH_3), 4.08 (d, 2H, J = 6.3 Hz, $NHC\underline{H}_2$), 7.12 (m, 2H, ArH phenyl), 7.19 (m, 1H, $N\underline{H}CH_2$), 7.50 (m, 1H, ArH quinoxaline), 7.57 (m, 1H, ArH quinoxaline), 7.72 (m, 1H, ArH quinoxaline), 7.95 (d, 2H, J = 9.0 Hz, ArH phenyl), 8.70 (d, 1H, J = 8.0 Hz, ArH quinoxaline), 10.58 (s, 1H, N$\underline{H}$). ^{13}C NMR (DMSO-d_6): 28.21, 51.60, 55.44, 78.23, 114.32, 121.71, 125.56, 126.48, 127.68, 127.80, 130.14, 130.82, 133.75, 140.93, 148.09, 155.83, 157.82, 169.40, 170.88. HRMS calculated for $C_{23}H_{25}N_6O_5$ $(M + H)^+$, 465.1886; found, 465.1901.

*Benzyl N-(4-[2-(4-Methoxyphenyl)-1-oxo-1H,2H-[1,2,4]triazolo-[4,3-a]quinoxalin-4-yl]carbamoylphenyl)carbamate (**13**).* 4-Amino-

2-(4-methoxyphenyl)-1,2,4- triazolo[4,3-*a*]quinoxalin-1-one (**1**) (0.06 mmol) was treated twice with a solution of 4-(benzyloxycarbonylamino)benzoic acid (**9**) (0.12 mmol), HATU (0.12 mmol), HOAt (0.12 mmol), and DIPEA (0.24 mmol) to give a pale yellow solid (30 mg) that contained the desired acylated product **13** along with starting material **1** (9:1 by analytical RP-HPLC). This material was therefore further purified by preparative RP-HPLC, to afford **13** (8 mg, 24% yield) as a pale yellow solid. ^{1}H NMR (DMSO-d_6): δ 3.79 (s, 3H, OCH_3), 5.20 (s, 2H, OCH_2), 7.09 (d, 2H, J = 9.4 Hz, ArH phenyl), 7.36−7.47 (m, 5H, ArH Cbz), 7.54 (m, 1H, ArH quinoxaline), 7.62−7.66 (m, 3H, ArH quinoxaline, phenyl), 7.78 (d, 1H, J = 8.1 Hz, ArH quinoxaline), 7.88 (d, 2H, J = 8.7 Hz, ArH phenyl), 8.00 (d, 1H, J = 8.7 Hz, ArH quinoxaline), 10.20 (s, 1H, NH), 11.00 (s, 1H, NH). ^{13}C NMR (DMSO-d_6): δ 55.41, 66.12, 114.37, 117.32, 121.83, 126.08, 126.60, 126.71, 128.17, 18.24, 128.50, 129.68, 130.06, 131.72, 133.69, 136.34, 142.84, 143.19, 148.07, 153.24, 157.83, 165.61, 170.26, 170.89. HRMS calculated for $C_{31}H_{25}N_6O_5$ (M + H)$^+$, 561.1886; found, 561.1880. Analytical RP-HPLC R_t = 18.45 min.

General Procedure C: Synthesis of 14−16. To a solution of the Boc-protected compound **10**, **11**, or **12** in dichloromethane (1 mL) was added trifluoroacetic acid (1 mL), and the mixture was stirred for 1 h. The solvent was removed under reduced pressure to give the product (**14**, **15**, or **16**) as the trifluoroacetate salt in quantitative yield, which was then used without further purification.

*N-{2-[2-(2-Aminoethoxy)ethoxy]ethyl}-N′-[2-(4-methoxyphenyl)-1-oxo-[1,2,4]triazolo[4,3-a]quinoxalin-4-yl]succinamide (**14**).* *tert*-Butyl *N*-2-{2-[2-(3-{[2-(4-methoxyphenyl)-1-oxo-1*H*,2*H*-[1,2,4]-triazolo[4,3-*a*]quinoxalin-4-yl]carbamoyl}propanamido)ethoxy]-ethoxy}ethylcarbamate (**10**) (16 mg, 0.02 mmol) gave **14** (14 mg, quant.) as a pale green solid. $C_{26}H_{32}N_7O_6$ (M + H)$^+$, 538.2414; found, 538.2403. Analytical RP-HPLC R_t = 13.69 min.

*N-(8-Aminooctyl)-N′-[2-(4-methoxyphenyl)-1-oxo-1H,2H-[1,2,4]-triazolo[4,3-a]quinoxalin-4-yl]succinamide (**15**).* *tert*-Butyl *N*-8-(3-{[2-(4-methoxyphenyl)-1-oxo-1*H*,2*H*-[1,2,4]triazolo[4,3-*a*]-quinoxalin-4-yl]carbamoyl}propanamido)octylcarbamate (**11**) (6 mg, 0.009 mmol) gave **15** (5 mg, quant.) as a pale yellow solid. $C_{28}H_{36}N_7O_4$ (M + H)$^+$, 534.2829; found, 534.2819. Analytical RP-HPLC R_t = 15.60 min.

*2-Amino-N-[2-(4-methoxyphenyl)-1-oxo-1H,2H-[1,2,4]triazolo-[4,3-a]quinoxalin-4-yl]acetamide (**16**).* *tert*-Butyl *N*-([2-(4-methoxyphenyl)-1-oxo-1*H*,2*H*-[1,2,4]triazolo[4,3-*a*]quinoxalin-4-yl]-carbamoylmethyl)carbamate (**12**) (5 mg, 0.01 mmol) gave **16** (4 mg, quant.) as a pale yellow solid. $C_{18}H_{17}N_6O_3$ (M + H)$^+$, 365.1362; found, 365.1365. Analytical RP-HPLC R_t = 13.37 min.

*4-Amino-N-[2-(4-methoxyphenyl)-1-oxo-1H,2H-[1,2,4]triazolo-[4,3-a]quinoxalin-4-yl]benzamide (**17**).* A mixture of **13** and **1** (9:1 by RP-HPLC) (approximately 0.04 mmol of **13**) was dissolved in methanol/water/acetic acid (2 mL, 9:0.9:0.1) and 10% palladium-on-carbon (2 mg) was added. The flask was evacuated and filled with hydrogen (balloon) and stirred for 3 h. The reaction mixture was filtered through Celite, and the filtrate solvent was removed under reduced pressure to give a yellow solid (15 mg) that contained desired product **17** along with the starting impurity **1**. Two milligrams of this material was purified by semipreparative RP-HPLC to afford **17** (0.5 mg, 25%) as a pale yellow solid. HRMS calculated for $C_{23}H_{19}N_6O_3$ (M + H)$^+$, 427.1519; found, 427.1519. Analytical RP-HPLC R_t = 18.65 min.

General Procedure D: Synthesis of 18−23. A solution of amine **14** or **15** (2 equiv), DIPEA (4 equiv), and the fluorophore-SE (1 equiv) was stirred in DMF (1 mL) with the exclusion of light for 12 h. The solvent was removed under reduced pressure, and the residue was purified by semipreparative RP-HPLC.

*N-[2-(4-Methoxyphenyl)-1-oxo-1H,2H-[1,2,4]triazolo[4,3-a]-quinoxalin-4-yl]-N′-{8-[6-(2-{4-[(E)-2-(4,4-difluoro-4,4a-dihydro-5-(thiophen-2-yl)-4-bora-3a,4a-diaza-s-indacene-3-yl)ethenyl]-phenoxy}acetamido)hexanamido]octyl}succinamide (**18**).* BODIPY-630/650-SE (1.0 mg, 1.5 μmol) gave **18** (0.8 mg, 0.8 μmol, 75% yield) as a dark blue solid. $C_{57}H_{62}BF_2N_{10}O_7S$ (M + H)$^+$, 1079.4585; found, 1079.4498. Analytical RP-HPLC R_t = 24.53 min.

*{4-[(E)-2-(4,4-Difluoro-4,4a-dihydro-5-(thiophen-2-yl)-4-bora-3a,4a-diaza-s-indacene-3-yl)ethenyl]phenoxy}acetamido)-hexanamido]ethoxy}ethoxy)ethyl]succinamide (**19**).* BODIPY-630/650-SE (2.0 mg, 3.0 μmol) gave **19** (0.9 mg, 0.8 μmol, 28% yield) as a dark blue solid. $C_{55}H_{58}BF_2N_{10}O_9S$ (M + H)$^+$, 1083.4170; found, 1083.4175. Analytical RP-HPLC R_t = 22.30 min.

*N-[2-(4-Methoxyphenyl)-1-oxo-1H,2H-[1,2,4]triazolo[4,3-a]-quinoxalin-4-yl]-N′-(2-{2-[2-(6-{2-[4-(4,4-difluoro-4,4a-dihydro-5-(thiophen-2-yl)-4-bora-3a,4a-diaza-s-indacene-3-yl)phenoxy]-acetamido}hexanamido)ethoxy]ethoxy}ethyl)succinamide (**20**).* BODIPY-TR-SE (2.0 mg, 3.1 μmol) gave **20** (1.0 mg, 0.9 μmol, 29% yield) as a dark red solid. $C_{53}H_{56}BF_2N_{10}O_9S$ (M + H)$^+$, 1057.4014; found, 1057.3986. Analytical RP-HPLC R_t = 21.97 min.

*N-[2-(4-Methoxyphenyl)-1-oxo-1H,2H-[1,2,4]triazolo[4,3-a]-quinoxalin-4-yl]-N′-[2-(2-{2-[6-(2-2-[(1E,3E)-5-[(2E)-1-ethyl-3,3-dimethyl-5-sulfo-2,3-dihydro-1H-indol-2-ylidene]penta-1,3-dien-1-yl]-1-{5-[(2-{2-[2-(3-{[2-(4-methoxyphenyl)-1-oxo-1H,2H-[1,2,4]-triazolo[4,3-a]quinoxalin-4-yl]carbamoyl}propanamido)ethoxy]-ethoxy}ethyl)carbamoyl]pentyl}-3,3-dimethyl-3H-indol-1-ium-6-sulfonate (**21**).* Cy5-X-SE (1.0 mg, 1.3 μmol) gave **21** (0.7 mg, 0.8 μmol, 60% yield) as a bright blue solid. $C_{59}H_{70}N_9O_{13}S_2$ (M + H)$^+$, 1177.4534; found, 1177.4570. Analytical RP-HPLC R_t = 14.94 min.

2-[6-(Dimethylamino)-3-(dimethylimino)-3H-xanthen-9-yl]-5(4)-({5-[(2-{2-[2-(3-{[2-(4-methoxyphenyl)-1-oxo-1H,2H-[1,2,4]triazolo-[4,3-a]quinoxalin-4-yl]carbamoyl}propanamido)-ethoxy]ethoxy}-ethyl)carbamoyl]pentyl}carbamoyl)benzoate$^{mixed\ isomers}$ *(**22**).* TAMRA 5/6-X-SE (1.0 mg, 1.6 μmol) gave **22** (0.6 mg, 0.6 μmol, 38% yield) as a pink solid. An analytical RP-HPLC trace of the crude reaction mixture revealed only one peak that corresponded to the mass of **22**. This peak was collected by semipreparative RP-HPLC and analyzed by analytical RP-HPLC, which revealed only one symmetrical peak. Therefore, it was assumed that the purified **22** (0.6 mg) was a mixture of the 5- and 6-isomers. $C_{57}H_{64}N_{10}O_{11}$ (M + H)$^+$, 1064.4756; found, 1064.5231. Analytical RP-HPLC R_t = 16.42 min.

*2-[6-(Dimethylamino)-3-(dimethylimino)-3H-xanthen-9-yl]-5-((53-((2-(4-methoxyphenyl)-1-oxo-1,2-dihydro-[1,2,4]triazolo[4,3-a]quinoxalin-4-yl)amino)-39,50,53-trioxo-3,6,9,12,15,18,21,24,27,30,33,36,43,46-tetradecaoxa-40,49-diazatripentacontyl)carbamoyl)benzoate (**23**).* 5-TAMRA-PEG-SE (1.0 mg, 0.9 μmol) gave **23** (0.3 mg, 0.2 μmol, 22% yield) as a pink solid. $C_{78}H_{106}N_{10}O_{23}$ (M + 2H)$^+$, 775.3711; found, 775.3694. Analytical RP-HPLC R_t = 16.53 min.

General Pharmacology Methods: Generation of Constructs and Cell Lines Used and Cell Culture. CHO cells stably expressing a cAMP response element-secreted placental alkaline phosphatase (CRE-SPAP) reporter gene were transfected with cDNA encoding the human A_3AR using Lipofectamine (Invitrogen, Paisley, United Kingdom) according to the manufacturer's instructions. Cells were cultured under selection pressure in medium containing 1 mg/mL G418, and a clonal cell line was generated. These cells were used in the CRE-SPAP assay and for imaging. CHO cells stably expressing the A_1AR were as previously described[38] and used for the calcium flux assays and imaging. HEK293 cells stably expressing the Glosensor cAMP biosensor (Promega, United States) were used in the Glosensor cAMP assay. The sigSNAP-A_3AR construct was generated as follows; cDNA encoding the full-length human A_3AR, which did not contain a methionine start codon, was fused in frame with cDNA encoding a cell membrane localization signal sequence and the SNAP-tag (New England Biolabs, Ipswich, MA). DNA sequencing was carried out to confirm the sequence of the construct. To obtain a mixed population of sigSNAP-A_3AR-expressing cells, HEK293 cells were grown to 80% confluency in 75 cm^2 tissue culture flasks and then transfected with the sig-SNAP-A_3AR construct (10 mg/flask) in Optimem again using Lipofectamine according to the manufacturer's instructions. Successfully transfected cells were initially selected using medium containing 0.8 mg/mL Geneticin and subsequently cultured in 0.2 mg/mL Geneticin to maintain selection pressure. The CHO cell lines were maintained in Dulbecco's modified Eagle's medium (DMEM) nutrient mix F12 (DMEM/F12) supplemented with 10% fetal calf serum and 2 mM L-glutamine. The HEK293 cell lines were maintained in DMEM containing 10% fetal calf serum and 2 mM L-glutamine. All cell lines

were maintained at 37 °C in a humidified atmosphere of air/CO_2 (19:1).

CRE-SPAP Gene Transcription Assay. A_3AR CRE-SPAP cells were grown to confluence in clear 96-well plates. Cells were serum starved for 18 h prior to experiment. On the day of experiment, fresh serum-free medium (DMEM/F12 supplemented with 2 mM L-glutamine) was added to the cells, and three concentrations of test compound were added to the appropriate wells, and cells were incubated for 30 min at 37 °C/5% CO_2. After 30 min, increasing concentrations of the agonist NECA were added to the cells, and the cells were incubated for a further 30 min at 37 °C/5% CO_2, and then, 1 μM forskolin (FSK) was added to stimulate cAMP production within the cells. Cells were then incubated for a further 5 h. Following the 5 h incubation, all medium was removed from the cells, 40 μL of fresh serum-free medium was added to each well, and cells were incubated for a further 1 h at 37 °C/5% CO_2. The plates were then incubated at 65 °C for 30 min to destroy any endogenous alkaline phosphatases. Plates were cooled to room temperature, and 100 μL of 5 mM 4-nitrophenyl phosphate in diethanolamine-containing buffer [10% (v/v) diethanolamine, 280 mM NaCl, 500 μM $MgCl_2$, pH 9.85] was added to each well; the plates were then incubated at 37 °C for 20 min. The absorbance at 405 nm was measured using a Dynex MRX plate reader (Chelmsford, MA).

Calcium Mobilization Assay. CHO-A_1AR cells[35] were grown to confluence in black-walled, clear-bottom 96-well plates. On the day of the experiment, medium was removed from each well and replaced with 100 μL of HEPES-buffered saline solution (HBSS; 25 mM HEPES, 10 mM glucose, 146 mM NaCl, 5 mM KCl, 1 mM $MgSO_4$, 2 mM sodium pyruvate, 1.3 mM $CaCl_2$, and 1.5 mM $NaHCO_3$) supplemented with 2.5 mM probenecid, 2.3 μM Fluo-4AM, and 0.023% Pluronic F-127. Cells were incubated with Fluo-4-containing buffer for at least 45 min at 37 °C in the dark. Cells were then washed twice in HBSS, fresh HBSS with 2.5 mM probenecid with or without antagonist was added to each well, and cells were incubated for a further 30 min at 37 °C in the dark. Plates were then loaded onto a multiwell fluormetric imaging plate reader (FlexStation; Molecular Devices, Sunnyvale, CA), and the fluorescence was measured (excitation, 485 nm; emission, 520 nm) every 1.52 s for 200 s. Either HBSS or HBSS with the required concentration of NECA was added at 15 s.

Glosensor cAMP Assay. HEK293 Glonsensor cells were grown to confluence in white-walled, clear-bottom 96-well plates coated with poly-L-lysine to allow the cells to adhere to the plate. On the day of the assay, medium was removed from each well and replaced with HBSS containing 3% v/v Glosensor cAMP reagent. Equilibration of the Glosensor reagent within the cells was achieved by incubating the cells for 2 h at 37 °C. Where required, antagonists were added after 1.5 h. The required concentration of NECA was added after 2 h, and luminescence was read on an EnVision plate reader (PerkinElmer, Waltham, MA) every 2 min for 60 min. The maximal luminescence read was used for analysis.

Confocal Microscopy. Cells were grown to approximately 80% confluency on 8-well Labtek chambered coverglasses (Nunc Nalgene) in their appropriate growth medium. For HEK293 cells, plates were coated with poly-D-lysine prior to seeding of cells. For CHO cell experiments, cells were washed twice in Hank's balanced salt solution (HBS) and then incubated in the presence or absence of 100 nM MRS1220 (CHO-A_3AR CRE-SPAP cells) or 100 nM DPCPX (CHO-A_1AR cells) for 30 min at 37 °C. Cells were then incubated with **19** or **20** at the required concentration for 10 min at room temperature, prior to collection of single equatorial confocal images. Images were obtained on a Zeiss LSM510 Meta NLO confocal microscope using a 40× c-Apochromat 1.2NA water-immersion objective. For **19**, images were collected using 633 nm excitation, a 488/561/633 dichroic and emission collected through a 650LP filter. For **20**, 561 nm excitation was used with the same dichroic, with emission collected using a LP575 filter. In each case, a pinhole diameter of 1 Airy Unit was used, and laser power, gain, and offset were kept the same for samples within each experiment.

For experiments on HEK293-SNAP-A_3AR cells, growth medium was removed, and cells were incubated in full growth medium containing 0.5 mM BG-AlexaFluor488 (New England Biolabs) for 15 min at 37 °C in a humidified atmosphere of air/CO_2 (19:1). Cells were subsequently washed three times in HBS, before incubation in the presence or absence of 100nM MRS1220 or PSB603 for 30 min at 37 °C. Cells were then incubated with 5 nM **19** for 10 min at room temperature, and confocal images were obtained as for CHO cells, except using dual excitation with 488 (BG-AlexaFluor488) and 633 nm (BODIPY 630/650) lasers. Light was directed to sample using a 488/561/633 primary dichroic, and emission split through an NFT565 secondary dichroic to two detection channels through BP500-530IR and BP650-710IR emission filters. The pinhole diameter was set to 1 Airy unit for 633 nm excitation, and that for the 488 nm channel was adjusted to match the slice depth. Again, laser powers and detector gains and offset were kept constant within individual experiments. Colocalization analysis was performed in Zeiss AIM4.2 software.

In both cases, images are presented as representative of an individual experiment with matched conditions. Linear adjustments to image brightness and contrast have been applied equally across all comparative images using Zeiss AIM4.2 software to prepare images for presentation.

Data Analysis. All data were fitted using Prism5 (GraphPad Software, San Diego, CA). For the CRE-SPAP gene transcription assay, NECA concentration−response curves in the absence and presence of increasing concentrations of test compounds were globally fit to the following interaction model in Prism5.

$$\text{response} = \frac{E_{max} \times [A]}{\left([A] + EC_{50} \times \left(1 + \frac{[B]}{K_D}\right)\right)}$$

where E_{max} is the maximal response, EC_{50} is the molar concentration of NECA [A] in the absence of test compound required to generate a response that is 50% of E_{max}, [B] is the concentration of test compound, and K_D is the antagonist equilibrium dissociation constant. For the calcium mobilization and Glosensor experiments, estimated affinity values (pK_D) were calculated from the shift of the agonist concentration−response curves elicited in the presence of 1 μM antagonist using the following equation:

$$DR = 1 + \frac{[B]}{K_D}$$

where DR (dose ratio) is the ratio of the antagonist concentration required to stimulate an identical response in the presence and absence of antagonist, [B]. Where there was no significant shift in the agonist concentration−response curve in the presence of 1 μM antagonist, a pK_D of >6 is quoted.

AUTHOR INFORMATION

Corresponding Author

*Tel: +44-115-8230082. Fax: +44-115-8230081. E-mail: stephen.hill@nottingham.ac.uk (S.J.H.). Tel: +44-115-9513026. Fax: +44-115-9513412. E-mail: barrie.kellam@nottingham.ac.uk (B.K.).

Notes

The authors declare the following competing financial interest(s): B.K and S.J.H. are founding directors of the University of Nottingham spin-off company CellAura Technologies Ltd.

ACKNOWLEDGMENTS

This work was supported by the Medical Research Council, UK (Grant No. G0800006).

ABBREVIATIONS USED

AR, adenosine receptor; Boc, *tert*-butyl carbamate; BODIPY-X-630/650, 6-(((4,4-difluoro-5-(2-thienyl)-4-bora-3*a*,4*a*-diaza-*s*-

indacene-3-yl)styryloxy)acetyl)amino hexanoic acid; BODIPY-X-TR, 6-(((4-(4,4-difluoro-5-(2-thienyl)-4-bora-3*a*,4*a*-diaza-*s*-indacene-3-yl)phenoxy)acetyl)amino)hexanoic acid; BODIPY, bordifluoropyrromethene; cAMP, cyclic adenosine monophosphate; CBZ, benzyl carbamate; CHO, Chinese hamster ovary; CRE-SPAP, cyclic AMP response element promoted secreted placental alkaline phosphatase; Cy5-X, 3*H*-indolium,2-[5-[1-[6-[(2,5-dioxo-1-pyrrolidinyl)oxy]-6-oxohexyl]-1,3-dihydro-3,3-dimethyl-5-sulfo-2*H*-indol-2 ylidene]-1,3-pentadien-1-yl]-1-ethyl-3,3-dimethyl-5-sulfopotassium salt; DPCPX, 8-cyclopentyl-1,3-dipropylxanthine; FSK, forskolin; GPCR, G protein-coupled receptor; HATU, 2-(1*H*-7-azabenzotriazol-1-yl)-1,1,3,3-tetramethyluronoium hexafluorophosphate; HEK293, human embryonic kidney 293; HOAt, 1-hydroxy-7-azabenzotriazole; MRS1220, *N*-[9-chloro-2-(2-furanyl)[1,2,4]-triazolo[1,5-*c*]quinazolin-5-yl]benzene acetamide; NECA, adenosine-5-*N*-ethylcarboxamide; PEG, polyethylene glycol; PSB603, 8-[4-[4-(4-chlorophenzyl)piperazide-1-sulfonyl)-phenyl]]-1-propylxanthine; RP-HPLC, reversed-phase high pressure liquid chromatography; SE, succinimidyl ester; TAMRA-5/6-X, 6-(tetramethylrhodamine-5-(and-6)-carboxamido)hexanoic acid; XAC, xanthine amine congener

REFERENCES

(1) Lundstrom, K. H. Biology of G protein-coupled receptors. In *G Protein-Coupled Receptors in Drug Discovery*; Lundstrom, K. H., Chiu, M. L., Eds.; CRC Press: Boca Raton, FL, 2006; Vol. *4*, pp 3−14.

(2) Gessi, S.; Merighi, S.; Varani, K.; Leung, E.; Mac Lennan, S.; Borea, P. A. The A_3 adenosine receptor: An enigmatic player in cell biology. *Pharmacol. Ther.* **2008**, *117*, 123−140.

(3) Koscsó, B.; Csóka, B.; Pacher, P.; Haskó, G. Investigational A_3 adenosine receptor targeting argents. *Expert Opin. Invest. Drugs* **2011**, *20*, 757−768.

(4) Borea, P. A.; Gessi, S.; Bar-Yehuda, S.; Fishman, P. A_3 Adenosine receptor: Pharmacology and Role in Disease. *Handb. Exp. Pharmacol.* **2009**, *193*, 297−327.

(5) Müller, C. E.; Jacobson, K. A. Recent developments in adenosine receptor ligands and their potential as novel drugs. *Biochim. Biophys. Acta* **2011**, *1808*, 1290−1308.

(6) Avni, I.; Garzozi, H. J.; Barequet, I. S.; Segev, F.; Varssano, D.; Sartani, G.; Chetrit, N.; Bakshi, E.; Zadok, D.; Tomkins, O.; Litvin, G.; Jacobson, K. A.; Fishman, S.; Harpaz, Z.; Farbstein, M.; Bar-Yehuda, S.; Silverman, M. H.; Kerns, W. D.; Bristol, D. R.; Cohn, I.; Fishman, P. Treatment of dry eye syndrome with orally administered CF101: Data from a phase 2 clinical trial. *Ophthalmology* **2010**, *117*, 1287−1293.

(7) Cohen, S.; Stemmer, S. M.; Zozulya, G.; Ochaion, A.; Patoka, R.; Barer, F.; Bar-Yehuda, S.; Rath-Wolfson, L.; Jacobson, K. A.; Fishman, P. CF102 an A_3 adenosine receptor agonist mediates anti-tumor and anti-inflammatory effects in the liver. *J. Cell. Physiol.* **2011**, *226*, 2438−2447.

(8) Wan, T. C.; Ge, Z.-D.; Tampo, A.; Mio, Y.; Bienengraeber, M. W.; Tracey, W. R.; Gross, G. J.; Kwok, W.-M.; Auchampach, J. A. The A_3 adenosine receptor agonist CP-532,903 [N6-(2,5-dichlorobenzyl)-3′-aminoadenosine-5′-*N*-methylcarboxamide] protects against myocardial ischemia/reperfusion injury via the sarcolemmal ATP-sensitive potassium channel. *J. Pharmacol. Exp. Ther.* **2008**, *324*, 234−243.

(9) Okamura, T.; Kurogi, Y.; Hashimoto, K.; Sato, S.; Nishikawa, H.; Kiryu, K.; Nagao, Y. Structure-activity relationships of adenosine A_3 receptor ligands: New potential therapy for the treatment of glaucoma. *Bioorg. Med. Chem. Lett.* **2004**, *14*, 3775−3779.

(10) Gessi, S.; Merighi, S.; Sacchetto, V.; Simioni, C.; Borea, P. A. Adenosine receptors and cancer. *Biochim. Biophys. Acta* **2011**, *1808*, 1400−1412.

(11) Gessi, S.; Cattabriga, E.; Avitabile, A.; Gafa', R.; Lanza, G.; Cavazzini, L.; Bianchi, N.; Gambari, R.; Feo, C.; Liboni, A.; Gullini, S.; Leung, E.; Mac-Lennan, S.; Borea, P. A. Elevated expression of A_3 adenosine receptors in human colorectal cancer is reflected in peripheral blood cells. *Clin. Cancer Res.* **2004**, *10*, 5895−5901.

(12) Böhme, I.; Beck-Sickinger, A. G. Illuminating the life of GPCRs. *Cell Commun. Signal.* **2009**, *7*, 16−38.

(13) Jacobson, K. A. Functionalized congener approach to the design of ligands for G protein-coupled receptors (GPCRs). *Bioconjugate Chem.* **2009**, *20*, 1816−1835.

(14) Patel, H. H.; Murray, F.; Insel, P. A. G Protein-coupled receptor signaling components in membrane raft and caveolae microdomains. *Handb. Exp. Pharmacol.* **2008**, *186*, 167−184.

(15) Briddon, S. J.; Hill, S. J. Pharmacology under the microscope: the use of fluorescence correlation spectroscopy to determine the properties of ligand-receptor complexes. *Trends Pharmacol. Sci.* **2007**, *28*, 637−645.

(16) Cottet, M.; Faklaris, O.; Zwier, J. M.; Trinquet, E.; Pin, J.-P.; Durroux, T. Original Fluorescent Ligand-Based Assays Open New Perspectives in G Protein-Coupled Receptor Drug Screening. *Pharmaceuticals* **2011**, *4*, 202−214.

(17) Middleton, R. J.; Briddon, S. J.; Cordeaux, Y.; Yates, A. S.; Dale, C. L.; George, M. W.; Baker, J. G.; Hill, S. J.; Kellam, B. New fluorescent adenosine A_1-receptor agonists that allow quantification of ligand-receptor interactions in microdomains of single living cells. *J. Med. Chem.* **2007**, *50*, 782−793.

(18) Tosh, D. K.; Chinn, M.; Ivanov, A. A.; Klutz, A. M.; Gao, Z.-G.; Jacobson, K. A. Functionalized Congeners of A_3 Adenosine Receptor-Selective Nucleosides Containing a Bicyclo[3.1.0]hexane Ring System. *J. Med. Chem.* **2009**, *52*, 7580−7592.

(19) Briddon, S. J.; Middleton, R. J.; Cordeaux, Y.; Flavin, F. M.; Weinstein, J. A.; George, M. W.; Kellam, B.; Hill, S. J. Quantitative analysis of the formation and diffusion of A_1-adenosine receptor-antagonist complexes in single living cells. *Proc. Natl. Acad. Sci. U.S.A.* **2004**, *101*, 4673−4678.

(20) Baker, J. G.; Middleton, R.; Adams, L.; May, L. T.; Briddon, S. J.; Kellam, B.; Hill, S. J. Influence of fluorophore and linker composition on the pharmacology of fluorescent adenosine A_1 receptor ligands. *Br. J. Pharmacol.* **2010**, *159*, 772−786.

(21) Kecskés, M.; Kumar, T. S.; Yoo, L.; Gao, Z.-G.; Jacobson, K. A. Novel Alexa Fluor-488 labeled antagonist of the A_{2A} adenosine receptor: Application to a fluorescence polarization-based receptor binding assay. *Biochem. Pharmacol.* **2010**, *80*, 506−511.

(22) Kumar, T. S.; Mishra, S.; Deflorian, F.; Yoo, L. S.; Phan, K.; Kecskés, M.; Szabo, A.; Shinkre, B.; Gao, Z.-G.; Trenkle, W.; Jacobson, K. A. Molecular probes for the A_{2A} adenosine receptor based on a pyrazolo[4,3-*e*][1,2,4]triazolo[1,5-*c*]pyrimidin-5-amine scaffold. *Bioorg. Med. Chem. Lett.* **2011**, *21*, 2740−2745.

(23) Ulrich, G.; Ziessel, R.; Harriman, A. The chemistry of fluorescent bodipy dyes: Versatility unsurpassed. *Angew. Chem., Int. Ed.* **2008**, *47*, 1184−1201.

(24) Paoletta, S.; Federico, S.; Spalluto, G.; Moro, S. Receptor-driven identification of novel human A_3 adenosine receptor antagonists as potential therapeutic agents. *Methods Enzymol.* **2010**, *485*, 225−244.

(25) Colotta, V.; Catarzi, D.; Varano, F.; Cecchi, L.; Filacchioni, G.; Martini, C.; Trincavelli, L.; Lucacchini, A. 1,2,4-Triazolo[4,3-*a*]-quinoxalin-1-one: a versatile tool for the synthesis of potent and selective adenosine receptor antagonists. *J. Med. Chem.* **2000**, *43*, 1158−1164.

(26) Lenzi, O.; Colotta, V.; Catarzi, D.; Varano, F.; Filacchioni, G.; Martini, C.; Trincavelli, L.; Ciampi, O.; Varani, K.; Marighetti, F.; Morizzo, E.; Moro, S. 4-amido-2-aryl-1,2,4-triazolo[4,3-*a*]quinoxalin-1-ones as new potent and selective human A_3 adenosine receptor antagonists. Synthesis, pharmacological evaluation, and ligand-receptor modeling studies. *J. Med. Chem.* **2006**, *49*, 3916−3925.

(27) Colotta, V.; Catarzi, D.; Varano, F.; Lenzi, O.; Filacchioni, G.; Martini, C.; Trincavelli, L.; Ciampi, O.; Traini, C.; Pugliese, A. M.; Pedata, F.; Morizzo, E.; Moro, S. Synthesis, ligand-receptor modeling studies and pharmacological evaluation of novel 4-modified-2-aryl-1,2,4-triazolo[4,3-*a*]quinoxalin-1-one derivatives as potent and selective human A_3 adenosine receptor antagonists. *Bioorg. Med. Chem.* **2008**, *16*, 6086−6102.

(28) Baker, J. G.; Hall, I. P.; Hill, S. J. Agonist actions of "beta-blockers" provide evidence for two agonist activations sites or conformations of the human beta-1 adrenoceptor. *Mol. Pharmacol.* **2003**, *63*, 1312−1321.
(29) Cooper, J.; Hill, S. J.; Alexander, S. P. H. An endogenouse A_{2B} receptor coupled to cAMP generation in human embryonic kidney (HEK293) cells. *Br. J. Pharmacol.* **1997**, *122*, 546−550.
(30) Gautier, A.; Juillerat, A.; Heinis, C.; Correa, I. R.; Kindermann, M.; Beaufils, F.; Johnsson, K. An engineered protein tag for multiprotein labeling in living cells. *Chem. Biol.* **2008**, *15*, 128−136.
(31) Tahtaoui, C.; Parrot, I.; Klotz, P.; Guillier, F.; Galzi, J.-L.; Hibert, M.; Ilien, B. Fluorescent pirenzepine derivatives as potential bitopic ligands of the human M_1 muscarinic receptor. *J. Med. Chem.* **2004**, *47*, 4300−4315.
(32) Palczewski, K.; Kumasaka, T.; Hori, T.; Behnke, C. A.; Motoshima, H.; Fox, B. A.; Le Trong, I.; Teller, D. C.; Okada, T.; Stenkamp, R. E.; Yamamoto, M.; Miyano, M. Crystal Structure of Rhodopsin: A G Protein-Coupled Receptor. *Science* **2000**, *289*, 739−745.
(33) Jaakola, V.-P.; Griffith, M. T.; Hanson, M. A.; Cherezov, V.; Chien, E. Y. T.; Lane, J. R.; Ijzerman, A. P.; Stevens, R. C. The 2.6 angstrom crystal structure of a human A_{2A} adenosine receptor bound to an antagonist. *Science* **2008**, *322*, 1211−1217.
(34) Lebon, G.; Warne, T.; Edwards, P. C.; Bennett, K.; Langmead, C. J.; Leslie, A. G. W.; Tate, C. G. Agonist-bound adenosine A_{2A} receptor structures reveal common features of GPCR activation. *Nature* **2011**, 1−6.
(35) Doré, A. S.; Robertson, N.; Errey, J. C.; Ng, I.; Hollenstein, K.; Tehan, B.; Hurrell, E.; Bennett, K.; Congreve, M.; Magnani, F.; Tate, C. G.; Weir, M.; Marshall, F. H. Structure of the Adenosine A_{2A} Receptor in Complex with ZM241385 and the Xanthines XAC and Caffeine. *Structure* **2011**, *19*, 1283−1293.
(36) Song, H. Y.; Ngai, M. H.; Song, Z. Y.; Macary, P. A.; Hobley, J.; Lear, M. J. Practical synthesis of maleimides and coumarin-linked probes for protein and antibody labelling via reduction of native disulfides. *Org. Biomol. Chem.* **2009**, *7*, 3400−3406.
(37) Cinelli, M. A.; Cordero, B.; Dexheimer, T. S.; Pommier, Y.; Cushman, M. Synthesis and biological evaluation of 14-(aminoalkyl-aminomethyl)aromathecins as topoisomerase I inhibitors: Investigating the hypothesis of shared structure−activity relationships. *Bioorg. Med. Chem.* **2009**, *17*, 7145−7155.
(38) Cordeaux, Y.; Briddon, S. J.; Megson, A. E.; McDonnell, J.; Dickenson, J. M.; Hill, S. J. Influence of Receptor Number on Functional Responses Elicited by Agonists Acting at the Human Adenosine A_1 Receptor: Evidence for Signaling Pathway-Dependent Changes in Agonist Potency and Relative Intrinsic Activity. *Mol. Pharmacol.* **2000**, *58*, 1075−1084.